Membrane determinants for the passive translocation of analytes through droplet interface bilayers

Vincent Faugeras, Olivier Duclos, Didier Bazile, Abdou Rachid Thiam

Membrane determinants for the passive translocation of analytes through droplet interface bilayers

Vincent Faugeras[1,3], Olivier Duclos[2], Didier Bazile[3], Abdou Rachid Thiam[1]

[1]Laboratoire de Physique de l'École Normale Supérieure, ENS, Université PSL, CNRS, Paris, France

[2]Integrated Drug Discovery Platform. Sanofi R&D, Chilly-Mazarin, France.

[3]Pharmaceutics Development Platform. Sanofi R&D, Gentilly, France,

(correspondence to thiam@ens.fr)

Abstract

Understanding how small molecules cross cell membranes is crucial to pharmaceutics. Several methods have been developed to evaluate such a process, but they need improvement since many false-positive candidates are often selected. Robust tools enabling rapid and reproducible screening can increase confidence on hits, and artificial membranes based on droplet interface bilayers (DIBs) offer this possibility. DIBs consist in the adhesion of two phospholipid-covered water-in-oil droplets which reproduce a bilayer. By having donor and acceptor droplets, the permeability of an analyte can be studied. However, the relevance of this system relies on the comprehension of how well the physical chemistry of the produced bilayer recapitulates the behavior of cell membranes. This information is missing, and we address it here. Taking small fluorophores as model analytes, we studied their permeation through DIBs made of a wide range of phospholipids. We found that both the phospholipid acyl chain and polar head affect permeability. Overall, these parameters impact the phospholipid shape and thereupon the membrane lateral pressure, which is a major factor correlating with permeability in our system. These results depend on the nature of the chosen oil. We thereupon identified relevant physical chemistry conditions that best mimic the compactness and subsequent permeability of biological membranes.

Introduction

Oral delivery remains the most preferred route for drug administration.[1] However, it intrinsically limits the bioavailability of the drug, i.e. the fraction of the drug that enters the systemic circulation.[2] High bioavailability is a key requirement to increase chances for compounds to reach their target.[3] To meet such requirements, pharmaceutical industries have developed various *in vitro* and *in silico* methods to predict bioavailability at the very first stages in drug development.[4,5] The biopharmaceutics classification system was further introduced to categorize drugs based on their aqueous solubility and intestinal permeability, key parameters determining the rate of drug absorption and bioavailability.[6] Indeed, the permeability of intestine cells to a drug gives relevant clues on its *in vivo* bioavailability.[7]

Depending on the nature of the drug, transport through the intestine cells can take several forms, a passive one by diffusion across cell membranes or an active one via transporters or efflux systems.[8,9] For small molecules, transport is mainly achieved by passive diffusion, driven by the concentration gradient between the two sides of the semi-permeable cell membrane.[10]

A popular model system to study membrane permeability is cultured monolayers of Caco-2 cells (Figure 1.a), which are derived from small intestine cells and mimic the intestinal barrier.[11,12] This method cumulates contributions from both passive and active permeabilities, and diffusion through cell junctions, which cannot be decorrelated. Also, despite its biological relevance, this method is not suitable in its current form for high-throughput drug screening.[13]

The parallel artificial membrane permeability assay (PAMPA) was subsequently developed for the rapid study of the translocation of bioactive molecules. It is based on a filter plate made of pores, infused with a micrometer thick solution of phospholipids in oil, and placed between two aqueous compartments (Figure 1.a). PAMPA enables to screen and discriminate a wide range of compounds.[14] Albeit the presence of phospholipids, the water-oil-water film is distinct from phospholipid bilayer membranes.[15] The permeability of many compounds assessed by PAMPA was therefore discrepant from values measured by Caco-2 cells.[16,17]

Following the PAMPA approach, a drastic decrease or removal of the oil film would lead to the adhesion of the two phospholipid monolayers, thus reproducing more reliably a bilayer membrane. This is made possible by droplet interface bilayers (DIBs).[18,19] DIBs are formed between two water-in-oil droplets covered each by a phospholipid monolayer and paired by spontaneous adhesion, thereby reproducing a phospholipid bilayer membrane (Figure 1.a, c).[20,21] In this system, oil molecules might remain in the bilayer depending on the oil type and phospholipid composition, but the bilayer thickness remains at nanometric scale, close to the thickness of normal bilayers.[22–25] DIBs are advantageous because they can be generated in high throughput with a large range of physico-chemical conditions.[26] For instance, the permeability of solutes, ions, or water has been assessed using micropipette- or microfluidic-based DIBs.[27–30] Moreover, DIBs can be made with asymmetrical monolayers to study the

influence of membrane asymmetry on permeability.[31–34] Finally, the permeability of a wide range of hydrophilic and lipophilic drugs was estimated using hybrid planar droplet bilayers.[35,36] All these methods reveal the versatility of such systems for studying membrane permeation but, DIBs need to be considered as a complementary approach to Caco-2. Indeed, they cannot entirely recapitulate the intestinal environment and may not be suitable for studying active permeability. For the sake of using DIBs to assess permeability, it is necessary to reach a global knowledge of the physical properties of the produced bilayer so as to identify the best conditions mimicking the cell membrane. Such characterization is currently missing. Namely, the impact of the phospholipid composition and the surrounding oil phase on the permeability of solutes are needed to outperform the PAMPA method in terms of structural relevance and predictivity. Such consideration is necessary to level up the DIB method to closely mimic cellular bilayers and provide a rapid and more reliable permeability assessment of molecules. In this article, we explore the formation of DIBs under a variety of physico-chemical conditions and characterize the passive permeability of fluorophores, such as fluorescein, used as model analytes; these molecules, sized like small permeants, enable a readout of translocation by fluorescence. We found that both phospholipid acyl chain and polar head impact membrane permeability. These parameters essentially vary the intrinsic curvature of phospholipids, thereby altering the membrane lateral pressure which strongly correlated with membrane permeability in our system. This finding depends on the nature of the oil phase which modifies the nature and the thickness of the hydrophobic layer to be crossed. We thereupon identified relevant physical chemistry conditions for making DIBs that best mimic cell membrane with regard to permeation.

Results

Droplet pairing conditions and permeability determination.

With a fluidic device, donor and acceptor water droplets are separately generated in an oil phase, which contains phospholipids decorating the droplets interface (Figure 1.b). Binary droplets are then brought together off chip (Figure 1.c). When two water droplets are brought closer to each other, they spontaneously adhere due to the insolubility of the lipid surfactants in the solvent phase.[18,37] The adhesion process leads to the zipping of the phospholipid monolayers, hence forming a droplet interface bilayer (DIB).[19,38] Within a few minutes, the zipping process reaches an equilibrium state depending on the solvent and surfactants used.[21] Thus, we can follow the time course of transfer over an hour and determine bilayer permeability (Figure 1.c, d). During the permeation time course, the volume of the droplets and area of the patch were almost constant (Supplementary figure S1).

For the oil phase, we used glyceryl trioctanoate, belonging to triglycerides which are abundant in cells.[39] For surfactants, we chose a wide range of phospholipids with various polar heads and acyl chains, and mixtures thereof (Figure 2.a, b, c). Taking advantage of this diversity would enable to decipher key features that control membrane permeability.

For the analyte, we chose fluorophores as model molecules and opted for fluorescein and carboxyfluorescein, a carboxylated form of fluorescein. For the aqueous phase of both droplets, we used a biological buffer solution composed of 50 mM HEPES, 120 mM KAcetate, and 1 mM $MgCl_2$ in Milli-Q water (pH 7.4, 293 mOsm, I = 173 mM). This buffer of ~ 300 mOsm was unaffected by the added fluorophore at 250 µM, which represents less than 1 mOsmol. Thus, donor and acceptor droplets had the same osmolarity.

As a proof of principle, we made DIB constituted of DOPE phospholipid and found that fluorescein, unlike carboxyfluorescein, fully crossed the membrane within the same hour time course of permeation (Figure 1.c, d). In our buffer, at a pH of 7.4, fluorescein mainly bears two charges whereas carboxyfluorescein bears three. This is very likely the origin of their divergence in permeability as the energy barrier to cross the hydrophobic core of the bilayer increases with charge. Such discrepancy between the two dyes has already been reported.[29] We then focused on fluorescein to study how its permeability is altered by membrane composition.

The concentration of fluorescein in the acceptor droplet can be obtained from the conservation of mass: $C_{\mathrm{a}}V_a + C_{\mathrm{d}}V_d = C_{\mathrm{d0}}V_d$, where C is concentration and V is volume; “a” reporting for acceptor and “d” for donor compartment; C_{d0} is the concentration of the solute in the donor droplet at t_0, 250 µM. Since the concentration is proportional to the fluorescence intensity F, $C_{\mathrm{a}}/C_{\mathrm{d}} = F_{\mathrm{a}}/F_{\mathrm{d}}$, the mass conservation writes simply as: $C_{\mathrm{a}}V_a + C_{\mathrm{a}}(\frac{F_{\mathrm{d}}}{F_{\mathrm{a}}})V_d = C_{\mathrm{d0}}V_d$, which yields:

$$\frac{C_{\mathrm{a}}}{C_{\mathrm{d0}}} = \frac{V_{\mathrm{d}}}{V_{\mathrm{a}} + \frac{V_{\mathrm{d}} \,.\, F_{\mathrm{d}}}{F_{\mathrm{a}}}}$$

Note that here, the bleaching effects are irrelevant since we consider the ratio of solute concentrations, and that both acceptor and donor droplets are similarly bleached. On the other hand, the mass conservation and Fick's law give $C_a(t)/C_{d0} = Ce^{-\mu t} + \frac{b}{\mu}$, where $\mu = \frac{PA(V_{\mathrm{a}}+V_{\mathrm{d}})}{V_{\mathrm{a}}V_{\mathrm{d}}}$, A being the membrane area and P the membrane permeability (Figure 1.d).[40,41] Thus, by measuring the fluorescence signal of the acceptor and donor droplets over time (Supplementary Figure S2a,b), the evolution of the concentration in the acceptor droplet $C_a(t)/C_{d0}$ is known. We fit this concentration with the above exponential equation (Figure 1.d, Supplementary figure S2.b, c) and extract the parameter μ which gives the permeability value (Figure 1.d).

Permeability is increased by acyl chain unsaturation and altered by polar heads.

We first studied PE of various acyl chains, with an increasing number of unsaturation, 1 for POPE, 2 for DOPE and 4 for PufaPE and fully saturated chains for DPPE (Figure 2.a). Making stable DPPE DIBs in the time scale of permeability was not possible which is why we opted for studying it in DOPE/DPPE mixtures which enabled stable DIBs. We found that increasing the number of unsaturation significantly increased permeability, from $0{,}81.10^{-5}$ cm.s^{-1} for POPE, to $1.6.10^{-5}$ cm.s^{-1} for DOPE, and $6.5.10^{-5}$ cm.s^{-1} for PufaPE (Figure 2.d). In contrast, we did not observe a significant difference in permeability for 3:1 and 1:1 ratios of DOPE:DPPE mixtures (Figure 2.e). Note that the diffusion of the fluorophore in the droplet volume ~ 4.10^{-6} cm^2.s^{-1} is much faster than its above permeation kinetics, meaning that the unstirring of the water layer close to the bilayer is irrelevant with regard to permeation.[42,43]

We then studied the bilayer permeability of PE/PC mixtures (Figure 2.b). We systematically noticed a decreased permeability with the addition of PC (Figure 2.f). Permeability significantly decreased as the amount of POPC increased in POPC/DOPE mixtures, from $1.6.10^{-5}$ to $1.5.10^{-5}$ and $8.0.10^{-6}$ cm.s^{-1}, for 0 to 20 and 40 mol% of POPC. Likewise, DOPC addition significantly decreased permeability, down to $1.4.10^{-5}$ cm.s^{-1} for 25 mol% and to $1.2.10^{-5}$ cm.s^{-1} for 50 mol% of added DOPC (Figure 2.f). POPC decreased permeability more than DOPC. Permeation across DOPE/DPPC bilayers was similar to that across DOPE/DPPE. DPPC addition did not significantly change permeability.

We also studied the effect of cholesterol and negatively charged phospholipids such as PA and PS on bilayer permeability (Figure 2.c, g). The addition of cholesterol did not significantly change bilayer permeability. However, this might result from a difference in the adsorption of cholesterol and DOPE at the oil-water interface, as both were added from the oil phase. In such a case, the generated DIB bilayer composition would not be representative of the bulk

concentration. Compared with pure DOPE, negatively charged phospholipids significantly increased the permeability up to $2.1.10^{-5}$ cm.s^{-1} for DOPA and $4.2.10^{-5}$ cm.s^{-1} for DOPE/DOPS mixture at 1:1 (Figure 2.g), which was here the maximum DOPS concentration that enabled stable DIB in the time scale of permeation.

Permeability is strongly altered by unusual phospholipids with contrasted structure.

Our above results show that the nature of the acyl chains modulates permeability, namely permeation is increased by unsaturation (Figure 2.d). We decided to further test this by using synthetic phosphatidylcholine DPhPC and Pufa²PC which are uncommon phospholipids with very contrasted structures, both with symmetric acyl chains, methylated or fully unsaturated respectively (Figure 3.a). DPhPC is often used to prepare DIBs because it offers high membrane stability with no detectable gel to liquid crystalline phase transition.[44] Pufa²PC is also able to form flexible and stable bilayers.[45] Compared with PE phospholipids, DPhPC and Pufa²PC altered permeability very differently (Figure 3.b). We noticed an order of magnitude difference between these two phospholipids with a permeability of 0.75 10^{-5} cm.s^{-1} for DPhPC and of 9.0 10^{-5} cm.s^{-1} for Pufa²PC (Figure 3.b). Pufa²PC yielded the highest permeability to fluorescein of studied DIBs, similarly to other observations made when using giant unilamellar vesicles.[46] We thus tested whether it would increase the permeability to carboxyfluorescein, which did not cross PE DIBs (Figure 1.d). Permeation was still abolished, suggesting again a strong energy barrier for caboxyfluorescein to cross the bilayer, probably because of its additional charge (Supplementary figure S3).

The bulk oil phase modulates permeability.

Our goal is to identify the physico-chemical conditions of DIBs that best mimic cell membrane permeability. So far, we used glyceryl trioctanoate and wanted to determine if the nature of the oil impacts permeability. In fact, oil molecules can be trapped in the DIB bilayer to a level dependent on the oil type and the phospholipid composition.[23,24] Permeability could thus depend on the oil type.

We made DIBs with squalene oil, a cholesterol derivative which can be found abundant in specific cells, especially of skins, plants of fishes.[47] Permeation through squalene DIB was slower than trioctanoate, suggesting that it somehow increased the energy cost for translocating through the bilayer. Due to this slow permeation, fitting the one-hour permeation with a standard diffusion profile was not possible. For comparison purposes, we instead decided to consider the rate of translocation at 15 min, p_c, which enables a good appreciation of the difference in permeation between the two oils (Figure 3.c, d). Compared with trioctanoate, permeability significantly decreased with squalene by a three- and two-fold reduction for DOPE and DPhPC respectively (Figure 3.d). Interestingly, the permeability

between DOPE and DPhPC, which are structurally very different phospholipids, is significantly different for trioctanoate whilst similar for squalene.

DIBs made in squalene are reported to be thicker than triglyceride-based bilayers.[48] The increase in membrane thickness for squalene could thus decrease the permeability for DOPE and DPhPC. However, in our experimental set up, permeability does not necessarily correlate exclusively with thickness since PE DIBs, bearing more oil than PC DIBs[49], are probably thicker while being more permeable than PC DIBs. Thus, other factors rather than thickness alone also influenced permeability. Based on the solubility diffusion model, permeability would also dependon the partition coefficient of the solute $K,$ between the aqueous phase and the membrane, composed of phospholipids and oils.[41] Here, squalene could have a predominant contribution to the partition coefficient as compared with phospholipids, so that it took control over permeability, on the contrary to trioctanoate (Figure 3.d). These data illustrate the importance of the oil choice while studying permeation with DIBs.

Membrane lateral pressure modulates the permeability of DIBs made in triglycerides.

Squalene seemed to mask the contribution of phospholipids in permeability, while trioctanoate did not (Figure 1d). Thus, we focused on trioctanoate to study how the permeability is varied by phospholipids. Following our above analysis, we posited that phospholipids would modulate the partition coefficient of the solute to the bilayer hydrophobic core. Indeed, phospholipids have different intrinsic curvatures, or shapes, meaning that their spacing in membrane can change. In other words, depending on the phospholipid type, the packing of the bilayer or its lateral pressure may vary [50]. Accordingly, the probability for solutes to reach the bilayer hydrophobic region also varies.

We decided to determine the relative lateral pressure π of a monolayer composing the bilayer, which is given by $\pi = \gamma_{m0} - \gamma_{mb}$, where γ_{mb} is the surface tension of a monolayer of the bilayer and γ_{m0} is that of the free standing water/oil interface saturated with phospholipids. This relative pressure compares the compaction of a DIB monolayer (related to γ_{mb}) relatively to the non-adhering monolayer counterpart (related to γ_{m0}). The tension of a monolayer in the bilayer can be inferred from the Young-Dupré equation which yields $\gamma_{mb} = \gamma_{m0}\big(cos(\theta)\big)$, where θ is the half contact angle between the droplets (Figure 1.d). The relative lateral pressure simply writes as $\pi = \gamma_{m0}\big(1 - cos(\theta)\big)$ and can be calculated by determining the initial monolayer tension and the DIB contact angle (an increase in this pressure translates a decrease of the bilayer tension, due to $cos(\theta)$). We measured these parameters for the studied lipid compositions (Figure 4.a, b, Supplement figure S4) and determined this pressure.

We reported the permeability for different phospholipid acyl chain and headgroup as a function of the relative lateral pressure and found a clear trend (Figure 4.c). For weaker lateral

pressures, e.g. beneath 1.5 $mN.m^{-1}$, the permeability is larger by one order of magnitude than for higher lateral pressures. Permeability plateaus above 2 $mN.m^{-1}$ in pressure. Compositions at the plateau are of higher lateral pressure, as for a bilayer membrane, and would thus match more biologically relevant physico-chemical situations; the permeability obtained for these conditions are in the range of values reported in the literature, between 0.5 10^{-6} $cm.s^{-1}$ and 1.7 10^{-5} $cm.s^{-1}$.[28,29,51–53] Our results suggest that bilayers made from trioctanoate and specific phospholipids, above 2 $mN.m^{-1}$ in lateral pressure, result in membranes with relevant permeability. In particular, it points out the bilayer compressibility as a determining factor for the passive permeability of solutes.

Discussion

DIBs are promising tools for screening molecules able to cross bilayer membranes.[28,29] However, their relevance depends on how closely they can mimic cell membranes, which is currently not well understood. To reach such knowledge, we probed the impact on permeability for a variety of phospholipid compositions, under given oil phases, so as to depict conditions that closely mimic the cell membrane permeability.

In trioctaonate DIBs, our data support that phospholipids alter the membrane lateral pressure that seems to be a major parameter controlling membrane permeability. Higher lateral pressures correspond to lower permeability. Based on the solubility diffusion model, the membrane permeability follows KD/d, where D is the diffusion coefficient across the phospholipid layers and d is the thickness of the latter[41]. PE DIBs bear more oil than PC DIBs, based on our previous work.[24] Thus, one could expect a slower diffusion coefficient D and a thicker membrane d in PE, which would both decrease permeability. Instead, a higher permeability was observed in PE as compared with PC. This finding indicates that the partition coefficient K may have been more affected in our system, at least for the above phospholipid conditions. More generally, by altering the DIB lateral pressure in the case of trioctanoate, phospholipids may particularly impact the partition coefficient of the solute.

The membrane lateral pressure depends on the phospholipids since varying acyl chains and headgroup overall alters the phospholipid shape, thereby impacting bilayer packing. The presence of unsaturation allows acyl chains to bend and to move along the phospholipid axis, resulting in a looser bilayer.[45] Accordingly, increasing unsaturation, e.g. from POPE to PufaPE or DPhPC to Pufa²PC, leads to leakier membranes (Figure 2.d, 3.b). Also, cone shaped lipids such as DOPE or DOPA loosen bilayers and hence lead to bilayers with a higher permeability than in PC whose cylindrical shape offers better bilayer packing.[54,55] However, DOPS which is also cylindrical, increased permeability compared with DOPE (Figure 2.g). High levels of DOPS, which is negatively charged, may have induced lateral phospholipid-phospholipid repulsions, which would result in a higher spacing of phospholipids, favorable for permeation.[56,57]

The nature of the oil phase influences DIB membrane permeability. Notably, we found that permeability is decreased by squalene (Figure 3.c, d), and even more by hexadecane (Supplementary figure S5). This discrepancy could be due to a difference in fluorescein partitioning between trioctanoate vs. squalene/hexadecane. In particular, trioctanoate has ester headgroups which offers the possibility to form hydrogen-bonds with solutes, which could significantly impact the partition coefficient.[58] Oils of similar nature such as squalene and hexadecane, which are hydrocarbons, could have similar partition coefficient. In this case, their

difference in permeability could come from a difference in DIB thickness for a given phospholipid composition. Indeed, the bilayer thickness decreases with increasing hydrocarbon length[23], which would promote less permeable hexadecane than squalene DIBs. This is in agreement with the low permeability values reported for fluorescein through hexadecane DIB, between 2.0 and $6.0.10^{-6}$ $cm.s^{-1}$,[28,29,53] lower than our results with squalene DIBs.

In conclusion, our study enables to get molecular insights on the permeability mechanism of solutes through DIBs. We identified physico-chemical conditions with a permeability of ~ 10^{-5} $cm.s^{-1}$ for fluorescein, similar to the permeability reported for this molecule in cells of rat jejunum or small intestine, ~ $0.4.10^{-5}$ $cm.s^{-1}$.[51,52] Our studies constitute an important step for further using DIBs to properly assay the passive translocation capacities of pharmaceutical molecules.

References

(1) Bardal, S. K.; Waechter, J. E.; Martin, D. S. *Applied Pharmacology*; Elsevier/Saunders, 2011.

(2) Waterbeemd, H. van de.; Testa, B. *Drug Bioavailability : Estimation of Solubility, Permeability, Absorption and Bioavailability*; Wiley-VCH, 2009.

(3) Van de Waterbeemd, H.; Testa, B. *The Why and How of Absorption, Distribution, Metabolism, Excretion, and Toxicity Research*; Elsevier Inc., 2013. https://doi.org/10.1016/B978-0-12-409547-2.02586-5.

(4) Lipinski, C. A.; Lombardo, F.; Dominy, B. W.; Feeney, P. J. Experimental and Computational Approaches to Estimate Solubility and Permeability in Drug Discovery and Development Settings. *Adv. Drug Deliv. Rev.* **2012**, *64* (1–3), 4–17. https://doi.org/10.1016/j.addr.2012.09.019.

(5) Thomas, V. H.; Bhattachar, S.; Hitchingham, L.; Zocharski, P.; Naath, M.; Surendran, N.; Stoner, C. L.; El-Kattan, A. The Road Map to Oral Bioavailability: An Industrial Perspective. *Expert Opin. Drug Metab. Toxicol.* **2006**, *2* (4), 591–608. https://doi.org/10.1517/17425255.2.4.591.

(6) Amidon, G. L.; Lennernäs, H.; Shah, V. P.; Crison, J. R. A Theoretical Basis for a Biopharmaceutic Drug Classification: The Correlation of in Vitro Drug Product Dissolution and in Vivo Bioavailability. *Pharm. Res. An Off. J. Am. Assoc. Pharm. Sci.* **1995**, *12* (3), 413–420. https://doi.org/10.1023/A:1016212804288.

(7) Usansky, H. H. Estimating Human Drug Oral Absorption Kinetics from Caco-2 Permeability Using an Absorption-Disposition Model: Model Development and Evaluation and Derivation of Analytical Solutions for Ka and Fa. *J. Pharmacol. Exp. Ther.* **2005**, *314* (1), 391–399. https://doi.org/10.1124/jpet.104.076182.

(8) Zhang, Y.; Benet, L. Z. The Gut as a Barrier to Drug Absorption. *Clin. Pharmacokinet.* **2001**, *40* (3), 159–168. https://doi.org/10.2165/00003088-200140030-00002.

(9) Pang, K. S. Modeling of Intestinal Drug Absorption: Roles of Transporters and Metabolic Enzymes (for the Gillette Review Series). *Drug Metab. Dispos.* **2003**, *31* (12), 1507–1519. https://doi.org/10.1124/dmd.31.12.1507.

(10) Daugherty, A. L.; Mrsny, R. J. Transcellular Uptake Mechanisms of the Intestinal Epithelial Barrier - Part One. *Pharm. Sci. Technol. Today* **1999**, *2* (4), 144–151. https://doi.org/10.1016/S1461-5347(99)00142-X.

(11) Yee, S. In Vitro Permeability across Caco-2 Cells (Colonic) Can Predict in Vivo (Small Intestinal) Absorption in Man - Fact or Myth. *Pharm. Res.* **1997**, *14* (6), 763–766. https://doi.org/10.1023/A:1012102522787.

(12) Van Breemen, R. B.; Li, Y. Caco-2 Cell Permeability Assays to Measure Drug Absorption. *Expert Opin. Drug Metab. Toxicol.* **2005**, *1* (2), 175–185.

https://doi.org/10.1517/17425255.1.2.175.

(13) Li, Y.; Shin, Y.; Yu, C.; Kosmeder, J.; Hirschelman, W.; Pezzuto, J.; van Breemen, R. Increasing the Throughput and Productivity of Caco-2 Cell Permeability Assays Using Liquid Chromatography-Mass Spectrometry: Application to Resveratrol Absorption and Metabolism. *Comb. Chem. High Throughput Screen.* **2003**, *6* (8), 757–767. https://doi.org/10.2174/138620703771826865.

(14) Kansy, M.; Senner, F.; Gubernator, K. Physicochemical High Throughput Screening: Parallel Artificial Membrane Permeation Assay in the Description of Passive Absorption Processes. *J. Med. Chem.* **1998**, *41* (7), 1007–1010. https://doi.org/10.1021/jm970530e.

(15) Avdeef, A.; Bendels, S.; Di, L. i.; Faller, B.; Kansy, M.; Sugano, K.; Yamauchi, Y. PAMPA—Critical Factors for Better Predictions of Absorption. *J. Pharm. Sci.* **2007**, *96* (11), 2893–2909. https://doi.org/10.1002/jps.21068.

(16) Hallifax, D.; Turlizzi, E.; Zanelli, U.; Houston, J. B. Clearance-Dependent Underprediction of in Vivo Intrinsic Clearance from Human Hepatocytes: Comparison with Permeabilities from Artificial Membrane (PAMPA) Assay, in Silico and Caco-2 Assay, for 65 Drugs. *Eur. J. Pharm. Sci.* **2012**, *45* (5), 570–574. https://doi.org/10.1016/j.ejps.2011.12.010.

(17) Wang, C. K.; Northfield, S. E.; Colless, B.; Chaousis, S.; Hamernig, I.; Lohman, R.-J.; Nielsen, D. S.; Schroeder, C. I.; Liras, S.; Price, D. A.; Fairlie, D. P.; Craik, D. J. Rational Design and Synthesis of an Orally Bioavailable Peptide Guided by NMR Amide Temperature Coefficients. *Proc. Natl. Acad. Sci.* **2014**, *111* (49), 17504–17509. https://doi.org/10.1073/pnas.1417611111.

(18) Poulin, P.; Bibette, J. Adhesion of Water Droplets in Organic Solvent. *Langmuir* **1998**, *14* (22), 6341–6343. https://doi.org/10.1021/la9801413.

(19) Bayley, H.; Cronin, B.; Heron, A.; Holden, M. A.; Hwang, W. L.; Syeda, R.; Thompson, J.; Wallace, M. Droplet Interface Bilayers. *Mol. Biosyst.* **2008**, *4* (12), 1191. https://doi.org/10.1039/b808893d.

(20) Thiam, A. R.; Bremond, N.; Bibette, J. Adhesive Emulsion Bilayers under an Electric Field: From Unzipping to Fusion. *Phys. Rev. Lett.* **2011**, *107* (6), 8–11. https://doi.org/10.1103/PhysRevLett.107.068301.

(21) Thiam, A. R.; Bremond, N.; Bibette, J. From Stability to Permeability of Adhesive Emulsion Bilayers. *Langmuir* **2012**, *28* (15), 6291–6298. https://doi.org/10.1021/la3003349.

(22) Mathai, J. C.; Tristram-Nagle, S.; Nagle, J. F.; Zeidel, M. L. Structural Determinants of Water Permeability through the Lipid Membrane. *J. Gen. Physiol.* **2008**, *131* (1), 69–76. https://doi.org/10.1085/jgp.200709848.

(23) Gross, L. C. M.; Heron, A. J.; Baca, S. C.; Wallace, M. I. Determining Membrane Capacitance by Dynamic Control of Droplet Interface Bilayer Area. *Langmuir* **2011**, *27* (23), 14335–14342. https://doi.org/10.1021/la203081v.

(24) Ben M'barek, K.; Ajjaji, D.; Chorlay, A.; Vanni, S.; Forêt, L.; Thiam, A. R. ER Membrane Phospholipids and Surface Tension Control Cellular Lipid Droplet Formation. *Dev. Cell* **2017**, *41* (6), 591-604.e7. https://doi.org/10.1016/j.devcel.2017.05.012.

(25) Chorlay, A.; Thiam, A. R. An Asymmetry in Monolayer Tension Regulates Lipid Droplet Budding Direction. *Biophys. J.* **2018**, *114* (3), 631–640. https://doi.org/10.1016/j.bpj.2017.12.014.

(26) Stanley, C. E.; Elvira, K. S.; Niu, X. Z.; Gee, A. D.; Ces, O.; Edel, J. B.; Demello, A. J. A Microfluidic Approach for High-Throughput Droplet Interface Bilayer (DIB) Formation. *Chem. Commun.* **2010**, *46* (10), 1620–1622. https://doi.org/10.1039/b924897h.

(27) Michalak, Z.; Muzzio, M.; Milianta, P. J.; Giacomini, R.; Lee, S. Effect of Monoglyceride Structure and Cholesterol Content on Water Permeability of the Droplet Bilayer. *Langmuir* **2013**, *29* (51), 15919–15925. https://doi.org/10.1021/la4040535.

(28) Nisisako, T.; Portonovo, S. A.; Schmidt, J. J. Microfluidic Passive Permeability Assay Using Nanoliter Droplet Interface Lipid Bilayers. *Analyst* **2013**, *138* (22), 6793–6800. https://doi.org/10.1039/c3an01314f.

(29) Schlicht, B.; Zagnoni, M. Droplet-Interface-Bilayer Assays in Microfluidic Passive Networks. *Sci. Rep.* **2015**, *5*, 1–8. https://doi.org/10.1038/srep09951.

(30) Elani, Y.; Solvas, X. C. I.; Edel, J. B.; Law, V.; Ces, O. Interface Bilayer Networks (Multisomes) and Their Use As Cell-Like Reactors. **2016**, 5961–5964. https://doi.org/10.1039/c6cc01434h.

(31) Hwang, W. L.; Chen, M.; Cronin, B.; Holden, M. A.; Bayley, H. Asymmetric Droplet Interface Bilayers. *J. Am. Chem. Soc.* **2008**, *130* (18), 5878–5879. https://doi.org/10.1021/ja802089s.

(32) Milianta, P. J.; Muzzio, M.; Denver, J.; Cawley, G.; Lee, S. Water Permeability across Symmetric and Asymmetric Droplet Interface Bilayers: Interaction of Cholesterol Sulfate with DPhPC. *Langmuir* **2015**, *31* (44), 12187–12196. https://doi.org/10.1021/acs.langmuir.5b02748.

(33) Li, X.; Huang, J.; Holden, M. A.; Chen, M. Peptide-Mediated Membrane Transport of Macromolecular Cargo Driven by Membrane Asymmetry. *Anal. Chem.* **2017**, *89* (22), 12369–12374. https://doi.org/10.1021/acs.analchem.7b03421.

(34) Taylor, G.; Nguyen, M. A.; Koner, S.; Freeman, E.; Collier, C. P.; Sarles, S. A. Electrophysiological Interrogation of Asymmetric Droplet Interface Bilayers Reveals Surface-Bound Alamethicin Induces Lipid Flip-Flop. *Biochim. Biophys. Acta - Biomembr.* **2019**, *1861* (1), 335–343. https://doi.org/10.1016/j.bbamem.2018.07.001.

(35) Lee, Y.; Lee, H. R.; Kim, K.; Choi, S. Q. Static and Dynamic Permeability Assay for Hydrophilic Small Molecules Using a Planar Droplet Interface Bilayer. *Anal. Chem.* **2018**, *90* (3), 1660–1667. https://doi.org/10.1021/acs.analchem.7b03004.

(36) Lee, Y.; Choi, S. Q. Quantitative Analysis for Lipophilic Drug Transport through a Model Lipid Membrane with Membrane Retention. *Eur. J. Pharm. Sci.* **2019**, *134*, 176–184. https://doi.org/10.1016/j.ejps.2019.04.020.

(37) Astafyeva, K.; Urbach, W.; Garroum, N.; Taulier, N.; Thiam, A. R. Stability of C12Ej Bilayers Probed with Adhesive Droplets. *Langmuir* **2015**, *31* (24), 6791–6796. https://doi.org/10.1021/acs.langmuir.5b00749.

(38) Huang, J.; Lein, M.; Gunderson, C.; Holden, M. a. Direct Quantitation of Peptide-Mediated Protein Transport across a Droplet–Interface Bilayer. *J. Am. Chem. Soc.* **2011**, *133* (40), 15818–15821. https://doi.org/10.1021/ja2046342.

(39) Martin, S.; Parton, R. G. Lipid Droplets: A Unified View of a Dynamic Organelle. *Nat. Rev. Mol. Cell Biol.* **2006**, *7* (5), 373–378. https://doi.org/10.1038/nrm1912.

(40) Flynn, G. L.; Yalkowsky, S. H.; Roseman, T. J. Mass Transport Phenomena and Models: Theoretical Concepts. *Journal of Pharmaceutical Sciences*. April 1974, pp 479–510. https://doi.org/10.1002/jps.2600630403.

(41) Nagle, J. F.; Mathai, J. C.; Zeidel, M. L.; Tristram-Nagle, S. Theory of Passive Permeability through Lipid Bilayers. *J. Gen. Physiol.* **2008**, *131* (1), 77–85. https://doi.org/10.1085/jgp.200709849.

(42) Barry, P. H.; Diamond, J. M. Effects of Unstirred Layers on Membrane Phenomena. *Physiological Reviews*. 1984, pp 763–872. https://doi.org/10.1152/physrev.1984.64.3.763.

(43) Casalini, T.; Salvalaglio, M.; Perale, G.; Masi, M.; Cavallotti, C. Diffusion and Aggregation of Sodium Fluorescein in Aqueous Solutions. *J. Phys. Chem. B* **2011**, *115* (44), 12896–12904. https://doi.org/10.1021/jp207459k.

(44) Lindsey, H.; Petersen, N. O.; Chan, S. I. Physicochemical Characterization of 1,2-Diphytanoyl-Sn-Glycero-3-Phosphocholine in Model Membrane Systems. *Biochim. Biophys. Acta - Biomembr.* **1979**, *555* (1), 147–167. https://doi.org/10.1016/0005-2736(79)90079-8.

(45) Manni, M. M.; Tiberti, M. L.; Pagnotta, S.; Barelli, H.; Gautier, R.; Antonny, B. Acyl Chain Asymmetry and Polyunsaturation of Brain Phospholipids Facilitate Membrane Vesiculation without Leakage. *Elife* **2018**, *7*, 1–23. https://doi.org/10.7554/elife.34394.

(46) Olbrich, K.; Rawicz, W.; Needham, D.; Evans, E. Water Permeability and Mechanical Strength of Polyunsaturated Lipid Bilayers. *Biophys. J.* **2000**, *79* (1), 321–327. https://doi.org/10.1016/S0006-3495(00)76294-1.

(47) Spanova, M.; Daum, G. Squalene - Biochemistry, Molecular Biology, Process

Biotechnology, and Applications. *Eur. J. Lipid Sci. Technol.* **2011**, *113* (11), 1299–1320. https://doi.org/10.1002/ejlt.201100203.

(48) Waldbillig, R. C.; Szabo, G. Planar Bilayer Membranes from Pure Lipids. *BBA - Biomembr.* **1979**, *557* (2), 295–305. https://doi.org/10.1016/0005-2736(79)90328-6.

(49) Ben M'barek, K.; Ajjaji, D.; Chorlay, A.; Vanni, S.; Forêt, L.; Thiam, A. R. ER Membrane Phospholipids and Surface Tension Control Cellular Lipid Droplet Formation. *Dev. Cell* **2017**, *41* (6), 591-604.e7. https://doi.org/10.1016/j.devcel.2017.05.012.

(50) Janmey, P. A.; Kinnunen, P. K. J. Biophysical Properties of Lipids and Dynamic Membranes. *Trends Cell Biol.* **2006**, *16* (10), 538–546. https://doi.org/10.1016/J.TCB.2006.08.009.

(51) Kristl, A. Membrane Permeability in the Gastrointestinal Tract: The Interplay between Microclimate PH and Transporters. *Chem. Biodivers.* **2009**, *6* (11), 1923–1932. https://doi.org/10.1002/cbdv.200900076.

(52) Berginc, K.; Žakelj, S.; Levstik, L.; Uršič, D.; Kristl, A. Fluorescein Transport Properties across Artificial Lipid Membranes, Caco-2 Cell Monolayers and Rat Jejunum. *Eur. J. Pharm. Biopharm.* **2007**, *66* (2), 281–285. https://doi.org/10.1016/j.ejpb.2006.10.023.

(53) Czekalska, M. A.; Kaminski, T. S.; Makuch, K.; Garstecki, P. Passive and Parallel Microfluidic Formation of Droplet Interface Bilayers (DIBs) for Measurement of Leakage of Small Molecules through Artificial Phospholipid Membranes. *Sensors Actuators, B Chem.* **2019**, 258–265. https://doi.org/10.1016/j.snb.2019.01.143.

(54) Zanghellini, J.; Wodlei, F.; von Grünberg, H. H. Phospholipid Demixing and the Birth of a Lipid Droplet. *J. Theor. Biol.* **2010**, *264* (3), 952–961. https://doi.org/10.1016/j.jtbi.2010.02.025.

(55) Thiam, A. R.; Farese, R. V.; Walther, T. C. The Biophysics and Cell Biology of Lipid Droplets. *Nat. Rev. Mol. Cell Biol.* **2013**, *14* (12), 775–786. https://doi.org/10.1038/nrm3699.

(56) Kooijman, E. E.; Chupin, V.; Fuller, N. L.; Kozlov, M. M.; De Kruijff, B.; Burger, K. N. J.; Rand, P. R. Spontaneous Curvature of Phosphatidic Acid and Lysophosphatidic Acid. *Biochemistry* **2005**, *44* (6), 2097–2102. https://doi.org/10.1021/bi0478502.

(57) Hirama, T.; Lu, S. M.; Kay, J. G.; Maekawa, M.; Kozlov, M. M.; Grinstein, S.; Fairn, G. D. Membrane Curvature Induced by Proximity of Anionic Phospholipids Can Initiate Endocytosis. *Nat. Commun.* **2017**, *8* (1). https://doi.org/10.1038/s41467-017-01554-9.

(58) Hannesschlaeger, C.; Horner, A.; Pohl, P. Intrinsic Membrane Permeability to Small Molecules. *Chem. Rev.* **2019**, *119* (9), 5922–5953. https://doi.org/10.1021/acs.chemrev.8b00560.

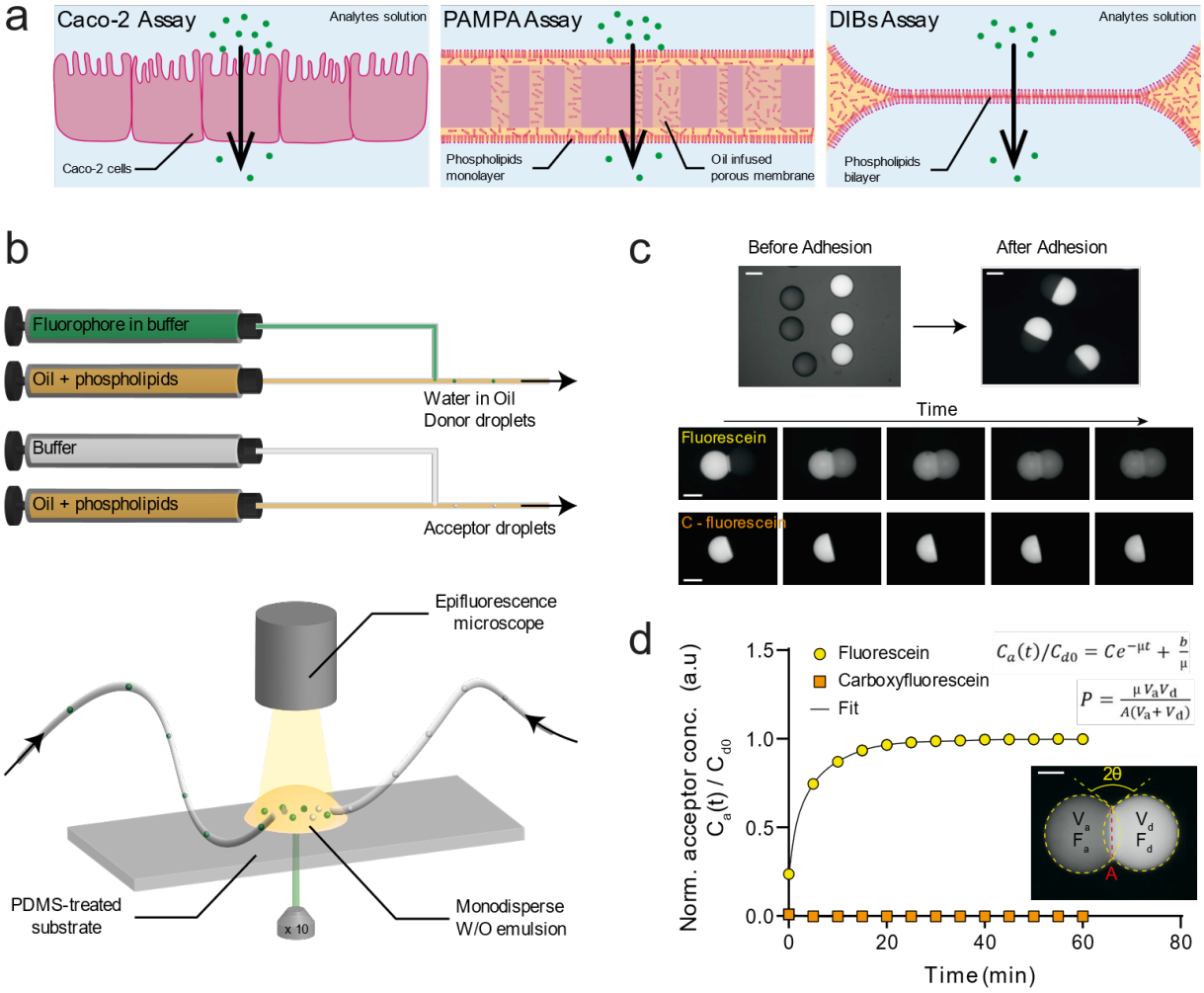

Figure 1: Passive permeability assay. (a) Schematic illustration of common *in vitro* assays used to assess membrane permeability, Caco-2 cells, PAMPA and DIBs. (b) Schematic of the proposed permeability assay. Two sets of W/O droplets, empty and analyte-filled (respectively acceptor and donor), are produced with a millifluidic device and dropped on a treated glass slide for monitoring under an epifluorescence microscope. (c) Top: examples of formed DIBs via droplet pairing off chip. Bottom, the passage of analyte (top: fluorescein; bottom: carboxyfluorescein) from the filled droplet to the empty one is followed over 60 minutes. Scale bars, 100 µm. (d) Permeation kinetics of fluorescein and carboxyfluorescein through glyceryl trioctanoate DOPE DIB; Permeability is calculated by fitting the curve of the acceptor concentration. Scale bars, 50 µm.

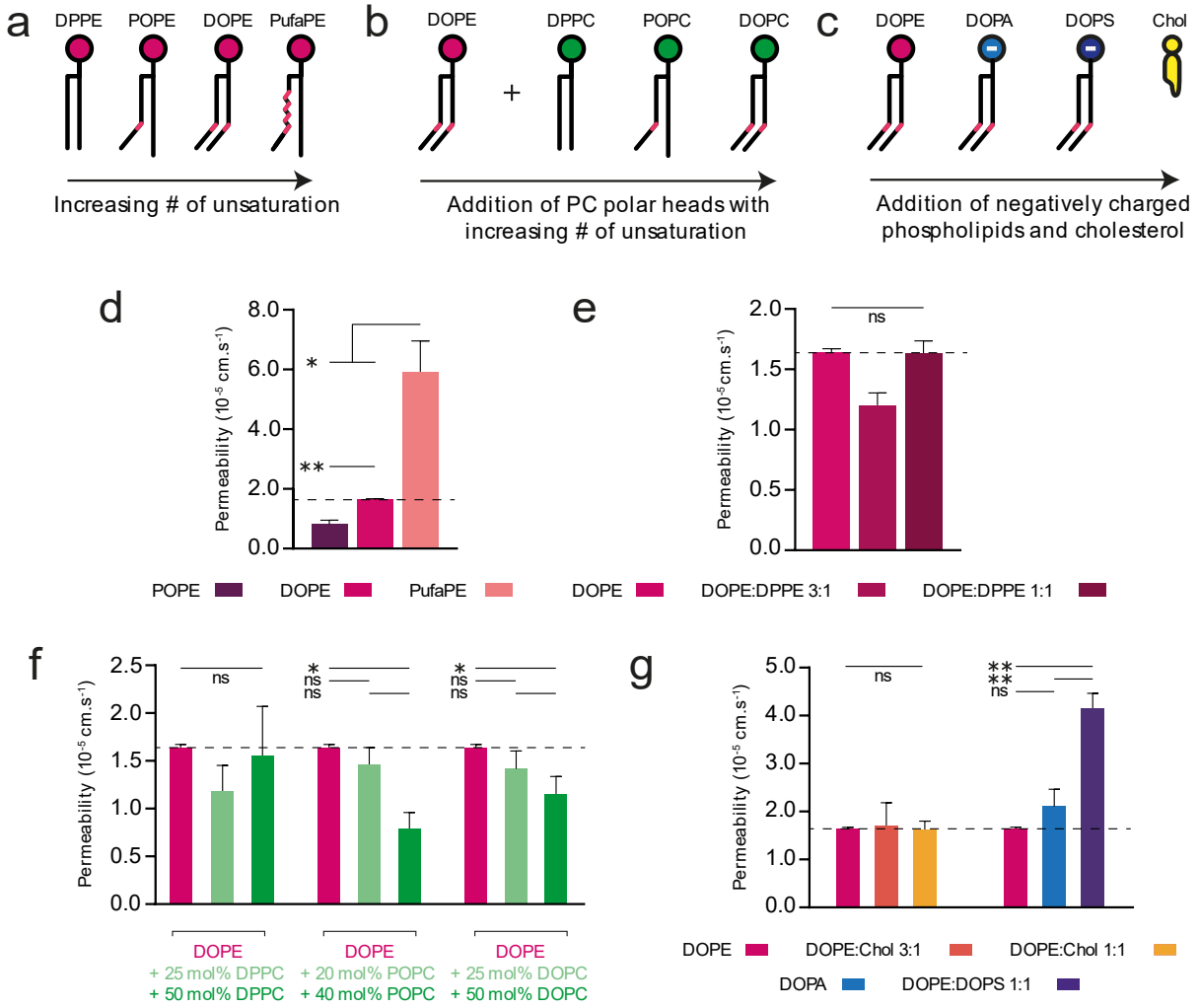

Figure 2: Permeability assay investigation through glyceryl trioctanoate DIB (analyte: fluorescein). (a)(b)(c) Phospholipids with various polar heads and acyl chains are studied. (d)(e)(f)(g) group phospholipids per nature. Permeability as a function of phospholipid compositions is represented (mean value, error bars represent the SD). ns indicates $p > 0.05$ not significant, * indicates $p < 0.05$, ** indicates $p < 0.01$.

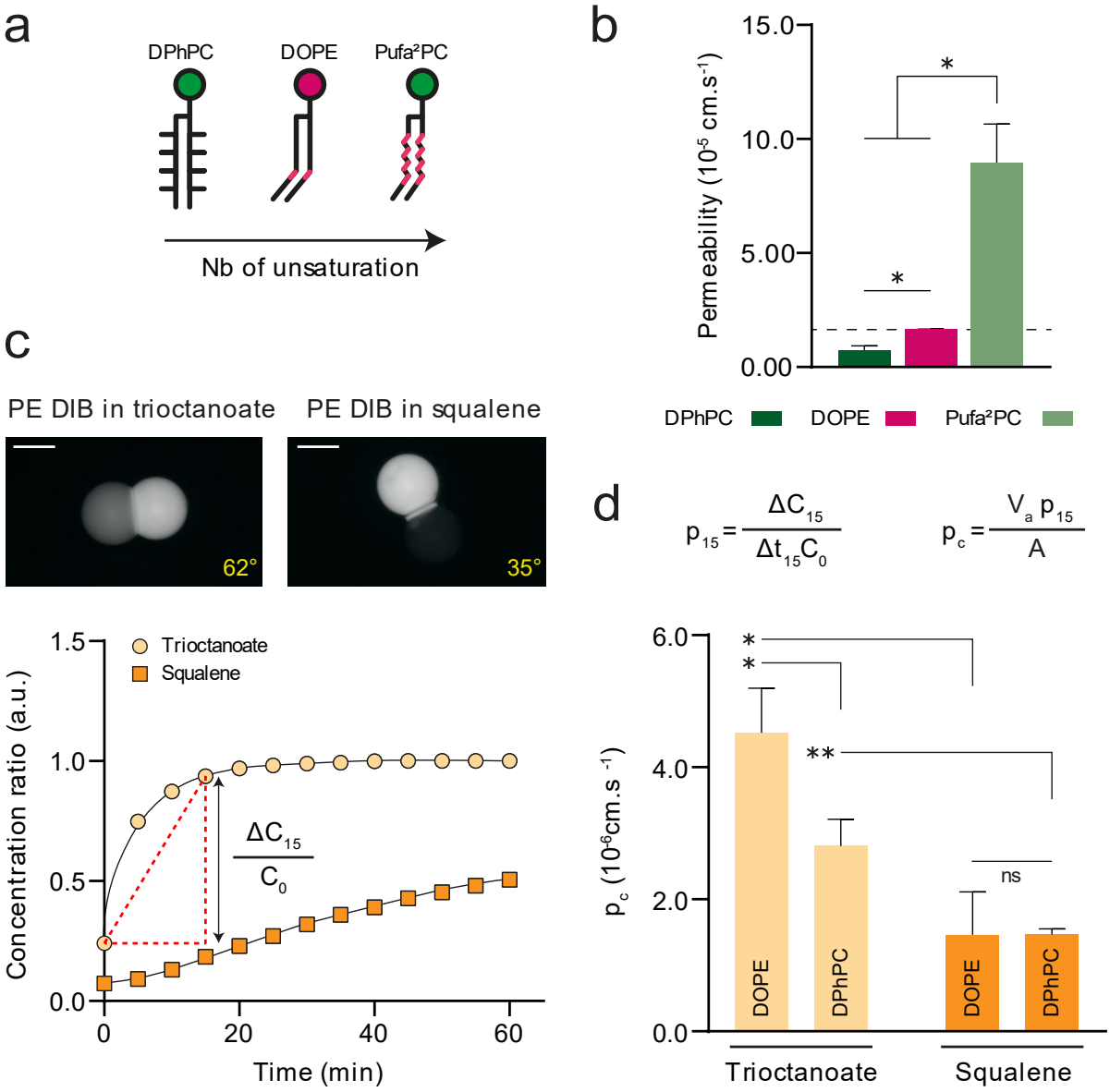

Figure 3: Impact of extreme phospholipids and of the oil on membrane permeability of fluorescein. (a) Diagram of rare symmetric phospholipids with either saturated or unsaturated acyl chains, displayed against DOPE. (b) Permeability as a function of phospholipid composition shown in (a). (c) Adhesion behavior of glyceryl trioctanoate and squalene DOPE DIBs (top). Permeation kinetics of analyte through DOPE DIBs depending on the oil composition. Scale bars, 100µm. (d) Introduction of permeation parameters p15 and pc which better describes slow permeation. Permeability as a function of oil nature and phospholipid compositions (mean value, error bars represent the SD). ns indicates $p > 0.05$ not significant, * indicates $p < 0.05$, ** indicates $p < 0.01$.

a

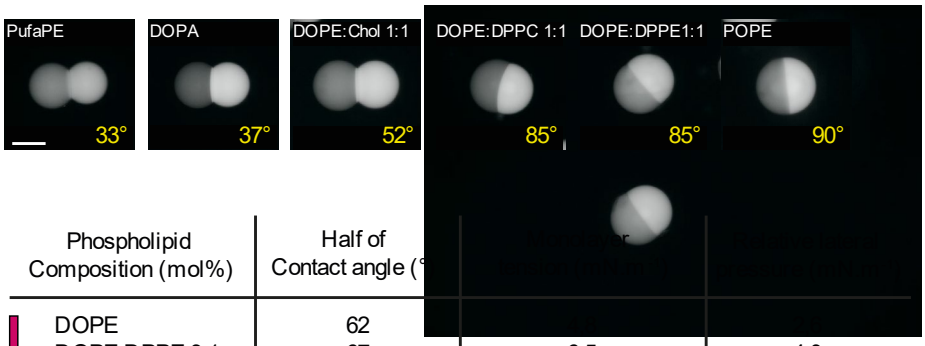

b

Phospholipid Composition (mol%)	Half of Contact angle (°		
DOPE	62		
DOPE:DPPE 3:1	67	6,5	4,0
DOPE:DPPE 1:1	80	5,7	4,7
POPE	90	7,4	7,4
PufaPE	33	5,3	0.9
DOPE:DOPC 3:1	56	3,9	1,7
DOPE:DOPC 1:1	85	3,7	3,4
DOPE:DPPC 3:1	60	4,9	2,5
DOPE:DPPC 1:1	85	4,2	3,8
DOPE:POPC 4:1	74	4,4	3,2
DOPE:POPC 3:2	85	3,6	3,3
DOPA	37	9,0	1,8
DOPE/DOPS 1:1	27	10,2	1,1
DOPE:Chol 3:1	50	5,5	2,0
DOPE:Chol 1:1	52	6,1	2,4
Pufa 20:4² PC	75	1,5	1,1
DPhPC	74	2,8	2,0

c

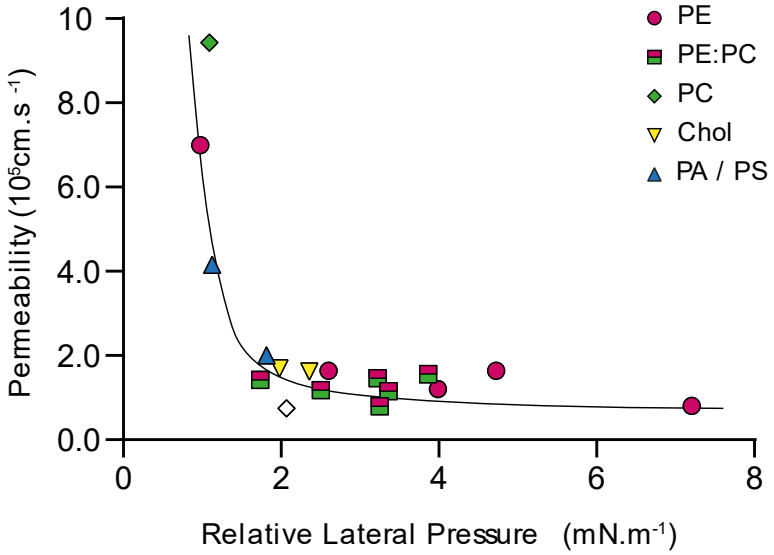

Figure 4: Influence of the bilayer physico-chemical state on the permeability. (a) DIB morphology as a function of the phospholipid composition. Scale bars, 100µm. (b) Measured contact angle (mean value ± 5°), monolayer tension (mean value ± 0,5 $mN.m^{-1}$) for every phospholipid composition studied, and the subsequently calculated relative pressure. (c) Permeability as a function of the relative lateral pressure of a monolayer composing the bilayer of DIBs. Purple/Green square: DOPE:DOPC, DOPC:DPPC and DOPE:POPC; green diamond: not natural PC, DPhPC and Pufa²PC.

Material and Method

Products. All phospholipids (Avanti Polar Lipids), glyceryl trioctanoate (Sigma-Aldrich), squalene (Sigma-Aldrich), hexadecane (Sigma-Aldrich), fluorescein sodium salt (VWR Chemicals), carboxyfluorescein (Sigma-Aldrich), HEPES (Sigma-Aldrich), potassium acetate KAcetate (Sigma-Aldrich) and magnesium chloride $MgCl_2$ (Sigma-Aldrich) are used without further purification.

Preparation of the Oil Phase. Phospholipids used for the oil phase are conditioned in chloroform. We first evaporate chloroform under a stream of argon; the dried lipids are subsequently re-solubilized to the desired concentration in the desired oil, notably glyceryl trioctanoate (TO) and squalene (SQ). Unless stated otherwise, a lipid concentration of 0.1 wt. % is used for all experiments, value above the critical concentration for every studied phospholipid composition.

Millifluidic setup to fabricate monodisperse W/O droplets. Unless mentioned otherwise, experiments are performed with a 0.1 wt. % lipids in oil solution and the following HKM buffer recipe: 50 mM HEPES, 120 mM KAcetate, and 1 mM $MgCl_2$ in Milli-Q water (at pH 7.4). For permeability assays, it is necessary to produce two types of droplets: acceptor droplets filled with buffer and donor droplets filled with a 250 µM solution of analyte in buffer. To do so, we use parallel circuits both composed of two Nemesys syringe pumps (Cetoni GmbH, Deutschland), one for the oil continuous phase and the other for the aqueous solution. The tubes (250 µm internal diameter) coming from the 1000 µL dispensing syringes (Gastight 1000 µL, Hamilton Company, US) are connected via a T-junction (IDEX Health & Science LLC, US) enabling the formation of W/O droplets. Flow rates for the oil and aqueous solution are respectively fixed at Q_O = 600 µL.h^{-1} and Q_W = 30 µL.h^{-1} resulting in about 150 µm diameter droplets. We finally placed the generated two families of droplets on a glass slide coated with PDMS (Figure 1.b).

Permeability Assay. All permeability assays are performed at room temperature T_{lab} = 21°C under an epifluorescence inverted microscope (Leica DM-IRB, Leica Microsystems SAS, France). Two droplets, one acceptor and one donor filled with analytes are selected. We then put the droplets in contact and a bilayer is formed spontaneously with a “zip-up” of monolayers. Just after DIB formation, we follow the passage of the analyte through the interface by taking pictures of the droplets every 5 minutes. The permeation is studied over 60 minutes (Figure 1.c, d).

Quantification of permeability. The analyte concentration is proportional to the fluorescence intensity. The initial concentration in the acceptor droplet is considered negligible, giving C_{a0} = 0 mol.L^{-1}, even though during the monolayer adhesion process a little fraction of solute can already translocate through the bilayer. Mass conservation equation is given by:

$$C_{\mathrm{a}}V_a + C_{\mathrm{d}}V_d = C_{\mathrm{d0}}V_d \qquad (1)$$

where $V_{a\ or\ d}$ and $C_{a\ or\ d}$ are respectively the volume and concentration of the acceptor and donor droplets; C_{d0} is the initial concentration of the donor droplet. We consider that throughout the permeation process, the volume and the patch area do not vary (see Supplement figure S1). Using the mass conservation and Fick's law[40,41], one gets:

$$\frac{d(C_a/C_{d0})}{dt} = -PA\left[\frac{1}{V_{\mathrm{a}}} + \frac{1}{V_{\mathrm{d}}}\right](C_a/C_{d0}) + P\frac{A}{V_{\mathrm{a}}} \qquad (2)$$

Where P is the permeability coefficient and A is the bilayer area. The resolution of this equation gives:

$$C_a(t)/C_{d0} = Ce^{-\mu t} + \frac{b}{\mu} \quad and \quad P = \frac{\mu V_{\mathrm{a}}V_{\mathrm{d}}}{A(V_{\mathrm{a}}+V_{\mathrm{d}})} \qquad (3)$$

The fit of our dataset with this exponential function gives access to the parameters μ, b, C and then permeability P.

We use the epifluorescence images of DIBs to measure the concentration of fluorescein in donor and acceptor droplets. As fluorescence intensity is proportional to concentration, we are able to study the evolution of the acceptor concentration (Supplementary figure S2). The concentration in the acceptor droplet is obtained from equation (1):
knowing that $C_{\mathrm{a}} = sF_{\mathrm{a}}$ and $C_{\mathrm{d}} = sF_{\mathrm{d}}$, where F denotes for the fluorescence intensity, one can write:

$$C_{\mathrm{a}}V_a + C_{\mathrm{a}}\left(\frac{F_{\mathrm{d}}}{F_{\mathrm{a}}}\right)V_d = C_{\mathrm{d0}}V_d$$

which yields

$$\frac{C_{\mathrm{a}}}{C_{\mathrm{d0}}} = \frac{V_{\mathrm{d}}}{V_{\mathrm{a}} + \frac{V_{\mathrm{d}}\,.\,F_{\mathrm{d}}}{F_{\mathrm{a}}}}$$

Note that $F_{\mathrm{d}}/F_{\mathrm{a}}$ annihilates the bleaching effect. By measuring the droplets' volume and intensity, the value of $C_{\mathrm{a}}/C_{\mathrm{d0}}$ is known. By fitting our dataset with an exponential equation (3), we can thus extract a permeation parameter « μ » and estimate the permeability of the bilayer. Each permeability value was determined by its mean and standard deviation. We performed a minimum of 3 measurements for each lipid condition.

Morphological analysis of DIBs. Compartment volumes $V_{a\ or\ d}$ are measured from a brightfield picture taken before droplet adhesion. Contact area A is obtained from the mean value of patch radius measured throughout the experiment. We also measure the contact angle robustly from droplets and patch radii with the following equation:

$$2\theta = sin^{-1}\left(\frac{R_p}{R_a}\right) + sin^{-1}\left(\frac{R_p}{R_d}\right)$$

where R_p and $R_{a\ or\ d}$ are respectively the radii of patch, acceptor and donor droplets.

Measurement of monolayer tension at a water/oil interface stabilized with phospholipids. Measurements are performed using a drop tensiometer device (Tracker, Teclis-IT Concept, France). The principle of the drop profile analysis is based on the determination of the shape of a liquid drop suspended in another liquid and its comparison with theoretical profiles calculated from the Gauss Laplace equation (Supplementary figure S4). In our case, the rising drop is the oil-containing lipid phase, dispersed in the aqueous buffer. Immediately after drop formation, the tension decreases along with the continuous inclusion of phospholipids at the oil/water interface. After a few minutes, the drop area and volume are maintained constant. Equilibrium surface tension is determined after 10 minutes. In the case of a slow adsorption, we extrapolate the curve with a theoretical experimental profile to get the equilibrium surface tension value γ_{eq} (Supplementary figure S4). Each surface tension was determined by a minimum of 3 independent measurements for each lipid condition studied.

Quantification and statistical analysis. Statistical significance is evaluated by Welch's t tests (unpaired parametric test, two-tailed P value) using Prism 8.0 (GraphPad Software, US). All values shown in the text and figures are mean ± S.D, and taken from at least 3 experiments (ns indicates $p > 0.05$ not significant, * indicates $p < 0.05$, ** indicates $p < 0.01$, *** indicates $p < 0.001$, **** indicates $p < 0.0001$).